Resource

Cell

Wireless Optofluidic Systems for Programmable In Vivo Pharmacology and Optogenetics

Graphical Abstract

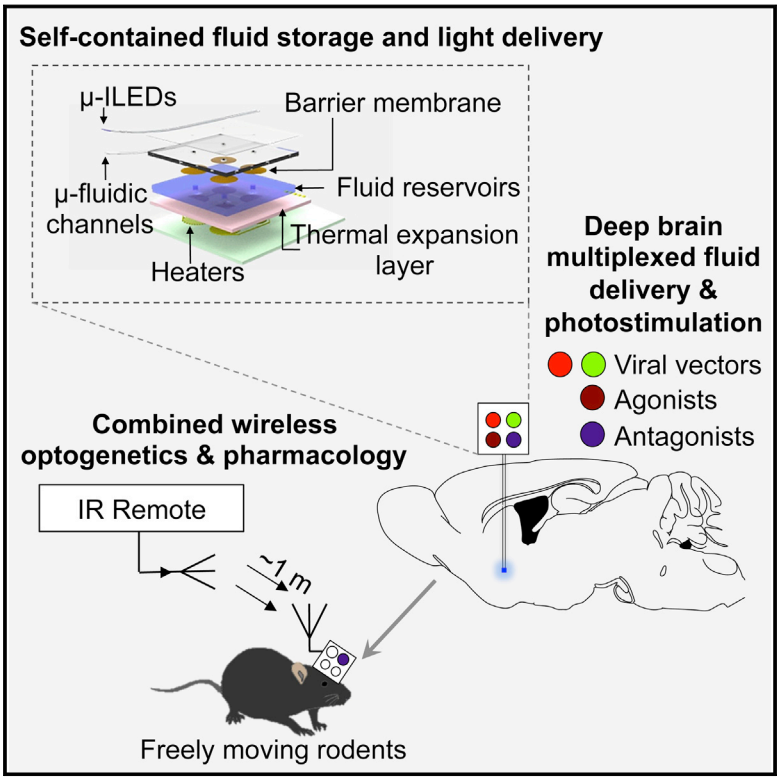

Highlights

- Neural probes with ultrathin, soft microfluidic channels coupled to μ-ILEDs
- Optofluidic probes minimize tissue damage and are suitable for chronic implants
- Wireless in vivo fluid delivery of viruses, peptides, and small-molecule agents
- Combined wireless optogenetics with pharmacology for neural circuit dissection

Authors

Jae-Woong Jeong, Jordan G. McCall, Gunchul Shin, ..., Yonggang Huang, Michael R. Bruchas, John A. Rogers

Correspondence

bruchasm@wustl.edu (M.R.B.), jrogers@uiuc.edu (J.A.R.)

In Brief

Ultrathin, flexible optofluidic neural probes enable wireless delivery of agents and optical manipulation in deep brain tissue of freely behaving animals. Combinatorial optogenetic, pharmacological, and viral approaches yield a powerful tool for in vivo dissection of neural circuitry.

Jeong et al., 2015, Cell *162*, 1–13
July 30, 2015
http://dx.doi.org/10.1016/j.cell.2015.06.058

CellPress

Please cite this article in press as: Jeong et al., Wireless Optofluidic Systems for Programmable In Vivo Pharmacology and Optogenetics, Cell (2015), http://dx.doi.org/10.1016/j.cell.2015.06.058

Cell

Wireless Optofluidic Systems for Programmable In Vivo Pharmacology and Optogenetics

Jae-Woong Jeong,[1,2,16] Jordan G. McCall,[3,4,5,16] Gunchul Shin,[2] Yihui Zhang,[6,7] Ream Al-Hasani,[3,4] Minku Kim,[2] Shuo Li,[2] Joo Yong Sim,[8] Kyung-In Jang,[2] Yan Shi,[6,9] Daniel Y. Hong,[3] Yuhao Liu,[2] Gavin P. Schmitz,[3] Li Xia,[3,10] Zhubin He,[6,11] Paul Gamble,[12] Wilson Z. Ray,[12] Yonggang Huang,[6] Michael R. Bruchas,[3,4,5,10,17,*] and John A. Rogers[2,13,14,15,17,*]

[1]Department of Electrical, Computer, and Energy Engineering, University of Colorado, Boulder, CO 80309, USA
[2]Department of Materials Science and Engineering, Beckman Institute for Advanced Science and Technology and Frederick Seitz Materials Research Laboratory, University of Illinois at Urbana-Champaign, Urbana, IL 61801, USA
[3]Department of Anesthesiology, Division of Basic Research, Washington University School of Medicine, St. Louis, MO 63110, USA
[4]Anatomy and Neurobiology, Washington University School of Medicine, St. Louis, MO 63110, USA
[5]Division of Biology and Biomedical Sciences, Washington University School of Medicine, St. Louis, MO 63110, USA
[6]Departments of Civil and Environmental Engineering and Mechanical Engineering, Center for Engineering and Health, Skin Disease Research Center, Northwestern University, Evanston, IL 60208, USA
[7]Center for Mechanics and Materials, Tsinghua University, Beijing 100084, China
[8]Bio-Medical IT Convergence Research Department, Electronics and Telecommunications Research Institute, Daejeon 305-700, Republic of Korea
[9]State Key Laboratory of Mechanics and Control of Mechanical Structures, Nanjing University of Aeronautics and Astronautics, Nanjing 210016, China
[10]Department of Biomedical Engineering, Washington University, St. Louis, MO 63130, USA
[11]School of Materials Science and Engineering, Harbin Institute of Technology, Harbin 150001, China
[12]Department of Neurosurgery, Washington University School of Medicine, St. Louis, MO 63110, USA
[13]Department of Electrical and Computer Engineering, University of Illinois at Urbana-Champaign, Urbana, IL 61802, USA
[14]Department of Mechanical Science and Engineering, University of Illinois at Urbana-Champaign, Urbana, IL 61802, USA
[15]Department of Chemistry, University of Illinois at Urbana-Champaign, Urbana, IL 61802, USA
[16]Co-first author
[17]Co-senior author
*Correspondence: bruchasm@wustl.edu (M.R.B.), jrogers@uiuc.edu (J.A.R.)
http://dx.doi.org/10.1016/j.cell.2015.06.058

SUMMARY

In vivo pharmacology and optogenetics hold tremendous promise for dissection of neural circuits, cellular signaling, and manipulating neurophysiological systems in awake, behaving animals. Existing neural interface technologies, such as metal cannulas connected to external drug supplies for pharmacological infusions and tethered fiber optics for optogenetics, are not ideal for minimally invasive, untethered studies on freely behaving animals. Here, we introduce wireless optofluidic neural probes that combine ultrathin, soft microfluidic drug delivery with cellular-scale inorganic light-emitting diode (μ-ILED) arrays. These probes are orders of magnitude smaller than cannulas and allow wireless, programmed spatiotemporal control of fluid delivery and photostimulation. We demonstrate these devices in freely moving animals to modify gene expression, deliver peptide ligands, and provide concurrent photostimulation with antagonist drug delivery to manipulate mesoaccumbens reward-related behavior. The minimally invasive operation of these probes forecasts utility in other organ systems and species, with potential for broad application in biomedical science, engineering, and medicine.

INTRODUCTION

Fundamental insights into the function of the central and peripheral nervous system often follow from advances in tools and methodologies for neuroscience research. Technologies for deep brain optical manipulation of neural activity allow for many types of basic research into neural circuits (Tye and Deisseroth, 2012), intracellular signaling (Siuda et al., 2015; Zhang and Cui, 2015), gene expression (Konermann et al., 2013; Polstein and Gersbach, 2015), and other biological processes. Additional levels of control follow from combined use of such approaches with pharmacological delivery (Jennings et al., 2013; Stamatakis et al., 2013; Walsh et al., 2014). Furthermore, the potential of these combinatorial approaches for clinical impact was recently demonstrated using combined optical and pharmacological intervention to inform and modify traditional, electrical deep brain stimulation to be more effective for off-label psychiatric disorders (Creed et al., 2015). A key technological challenge has been the development of miniaturized, self-contained systems that are capable of providing such functionality with wireless control in freely moving, awake animal models. Conventional methods rely on metal tubes (cannulas) and fiber optic cables to deliver drugs and light, respectively. Typically,

Please cite this article in press as: Jeong et al., Wireless Optofluidic Systems for Programmable In Vivo Pharmacology and Optogenetics, Cell (2015), http://dx.doi.org/10.1016/j.cell.2015.06.058

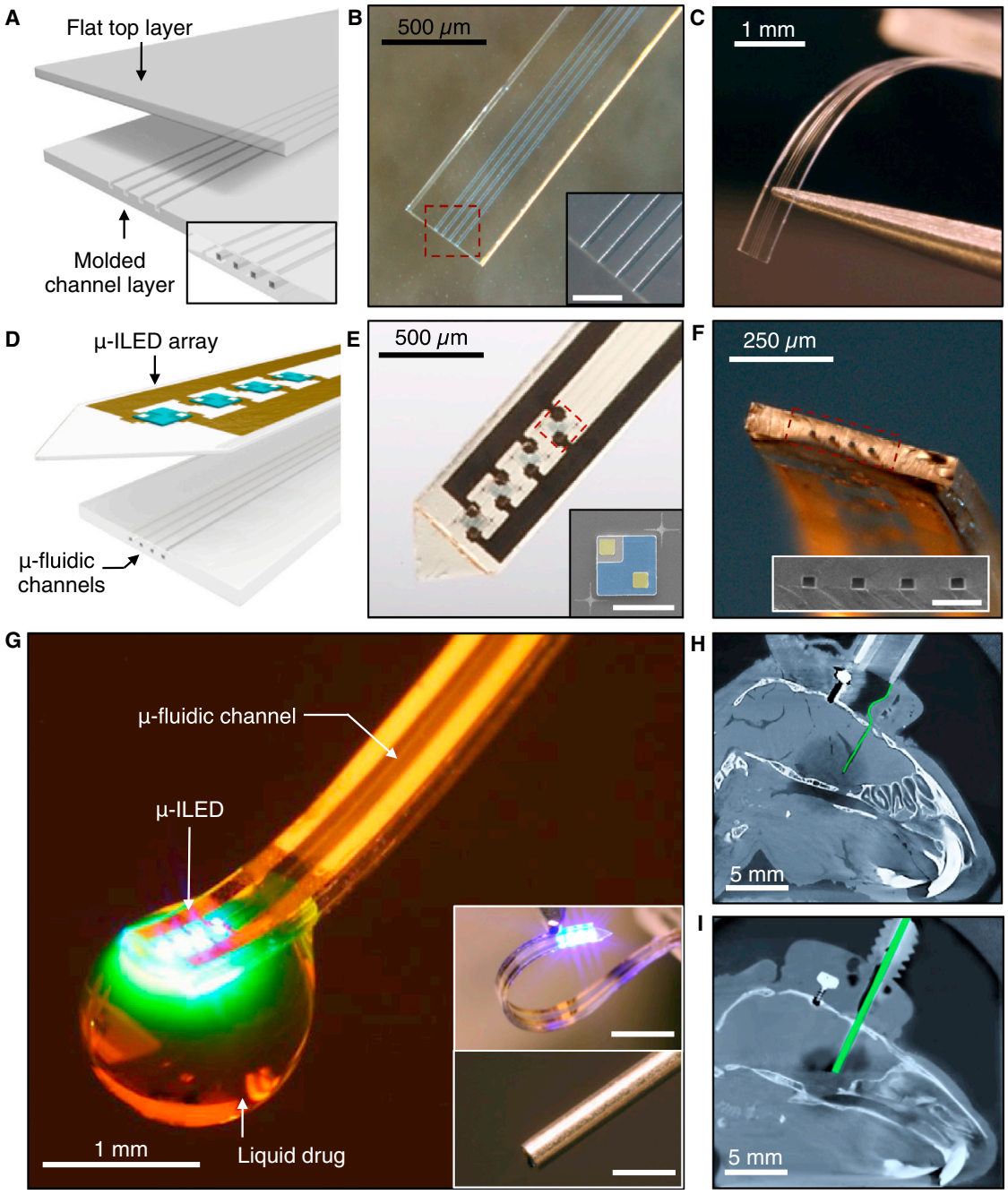

Figure 1. Ultrathin, Soft Neural Probes with Wireless Capabilities in Programmed Drug Delivery and Photostimulation

(A) Schematic diagram of the assembly of a soft microfluidic probe. Bonding thin, molded (bottom), and unmolded (top) layers of PDMS together yields a system that includes four separately addressable microfluidic channels, each with cross-sections of 10 × 10 μm^2 and a total thickness of 50 μm and width of 500 μm, as illustrated in the inset at the bottom right.

(B) Optical micrograph of a microfluidic probe formed in this way. (Inset) Magnified view of the channels. Scale bar, 100 μm.

(C) Picture that illustrates the soft, compliant mechanics of the device.

(D) Schematic diagram of the integration of a soft microfluidic probe with a flexible array of μ-ILEDs (each with lateral dimensions of 100 × 100 μm^2 and thicknesses of 6.54 μm) and metal interconnect traces on a film of PET (thickness of 6 μm).

(E) Optical micrograph of an integrated probe, which we refer to as an optofluidic system. (Inset) Colorized SEM of a representative μ-ILED (contact electrodes, yellow; spreading layer, blue). Scale bar, 100 μm.

(F) Tilted view of an optofluidic probe that shows the tip end. (Inset) SEM of the outlets of the microfluidic channels. Scale bar, 50 μm.

(legend continued on next page)

each modality requires connection to separately located light and fluid sources that physically tethers the animals and restricts their natural movement. Recent advances have combined cannulas and fiber optics into small, multifunctional fibers that have capabilities in fluid delivery and photostimulation but that retain similar requirements for multiple, external connections (Canales et al., 2015). All of these technologies use rigid materials as neural interfaces leading to adverse consequences for chronic use. The tissue benefit of mechanical compliance was recently demonstrated comparing standard systems against systems that combine soft electrodes and microfluidic structures in epidural implants (Minev et al., 2015) (see Table S1 for feature comparison).

The approach we report here describes complete platforms that include power supplies, control electronics, wireless interfaces, active fluidic handling systems, and efficient light sources into compact, head-mounted devices that interface with thin, mechanically compliant multifunctional neural probes. The result is a set of unique capabilities in programmed delivery of multiple types of pharmacological agents and monochromatic light to discretely targeted regions of the deep brain. These systems, which we refer to as wireless optofluidic neural probes, create important opportunities in neuroscience research that combine in vivo pharmacology with wireless optogenetics. Examples in awake, freely moving animals demonstrate the sophisticated levels of spatiotemporal control over neural circuit functions that are possible without physically contacting the animal. Specifically, optical manipulation of projections from the ventral tegmental area dopaminergic system into the nucleus accumbens can elicit place preference behaviors that can be blocked, in a temporally precise programmable manner, by site-specific infusion of a dopamine receptor antagonist. These and related studies represent the sort of versatile, complex experimental options provided by these optofluidic neural probes.

RESULTS

Ultrathin, Soft Neural Probes Have Wireless Capabilities for Programmed Drug Delivery and Photostimulation

Figures 1A–1C show schematic illustrations and photographs of a multichannel, soft microfluidic system in which two thin, narrow pieces of the elastomer polydimethylsiloxane (PDMS) bond together to form a set of four channels each with 10 × 10 μm^2 cross-sectional areas in a platform that has a total thickness of 50 μm (Figures S1A–S1C). These microfluidic probes (Figures 1B and 1C) are transparent (>95% throughout across wavelengths from 400 nm to 700 nm) and mechanically soft (modulus ~1 MPa; bending stiffness 13–18 N/m), thereby enabling both optical access and minimally invasive use in soft neural tissue (Canales et al., 2015; Capadona et al., 2012; Jeong et al., 2015; Kim et al., 2013b; Kozai et al., 2012; Minev et al., 2015; Subbaroyan et al., 2005; Wu et al., 2013). The former characteristic facilitates integration of microscale inorganic light-emitting diodes (μ-ILEDs) on a filament of polyethylene terephthalate (PET) with a thickness of 6 μm (Figure 1D). These μ-ILEDs (lateral dimensions of 100 × 100 μm^2 and 6.54 μm thick; Figure 1E) (Kim et al., 2013b) provide spatially and temporally precise delivery of light adjacent to the outlets of the microfluidic channels. Active infusion of multiple drugs through these four individual channels (Figure 1F) can be controlled independently from the μ-ILEDs. This system allows for tandem pharmacological and optogenetic manipulation of neural circuitry, with potential for application in optopharmacology where the use of light to activate compounds requires high spatiotemporal control of both drug and light delivery (Kramer et al., 2013) (Figure 1G and Movie S1).

Figures 1G, 1H, and 1I provide comparisons of this type of compliant optofluidic probe to a standard metal cannula (see also Figures S1D–S1H). The latter is hard, rigid, and displaces large amounts of brain tissue (diameter ~500 μm), whereas the former is soft, flexible, and minimally invasive (total thickness ~80 μm). The low bending stiffness (13–18 N/m, compared to >5 MN/m for the 26 gauge cannula) of the optofluidic probes (Figure S2A) facilitates adaptation to the micromotions associated with movement, respiration, and blood flow (Gilletti and Muthuswamy, 2006). This property minimizes mechanically induced damage or irritation of the brain tissue in chronic applications (Lee et al., 2005). X-ray computed tomographic images of mice implanted with these two types of fluidic delivery systems highlight the notable differences in scale and impact on the tissue (Figures 1H and 1I). Together, these optofluidic probes offer minimally invasive capabilities for combined fluid and photon delivery.

Thermo-Mechanical-Fluidic Characteristics of the Optofluidic Devices

Figure 2A presents a schematic diagram of the overall system with emphasis on the fluid-controlling hardware. The schemes for fluid handling and pumping represent extensions of recently reported drug delivery systems that use rigid, single-channel and single-reservoir microfluidics and wired control interfaces (Spieth et al., 2012). Each of the four channels connects to a separate reservoir whose base consists of an active layer (2:1 mixture of PDMS and expandable microspheres, Expancel 031 DU 40, AkzoNobel) that initiates pumping through expansion induced by Joule heating in an underlying element (serpentine traces of gold with thickness of 185 nm). The active layer increases in volume from thermally induced, irreversible expansion of hollow polymer microspheres that encapsulate hydrocarbon gas (Figure 2B). The supporting substrate (FR4) has low thermal conductivity (0.4 W/m·K), thereby minimizing the electrical power needed to reach the temperatures required for this type of thermal actuation. The four reservoirs exist as molded features in a cyclic olefin polymer (COP), chosen for its low water vapor permeability (0.023 g·mm/m^2·day). Thin copper

(G) Optofluidic neural probe during simultaneous drug delivery and photostimulation. (Insets) Comparison of such a device (top) and a conventional metal cannula (bottom; outer and inner diameters of ~500 and 260 μm, respectively). Scale bars, 1 mm.

(H and I) X-ray computed tomographic images of the mouse models with (H) an optofluidic neural probe and (I) a metal cannula implanted into the brain. Both devices are colorized green.

See also Figure S1 and Table S1.

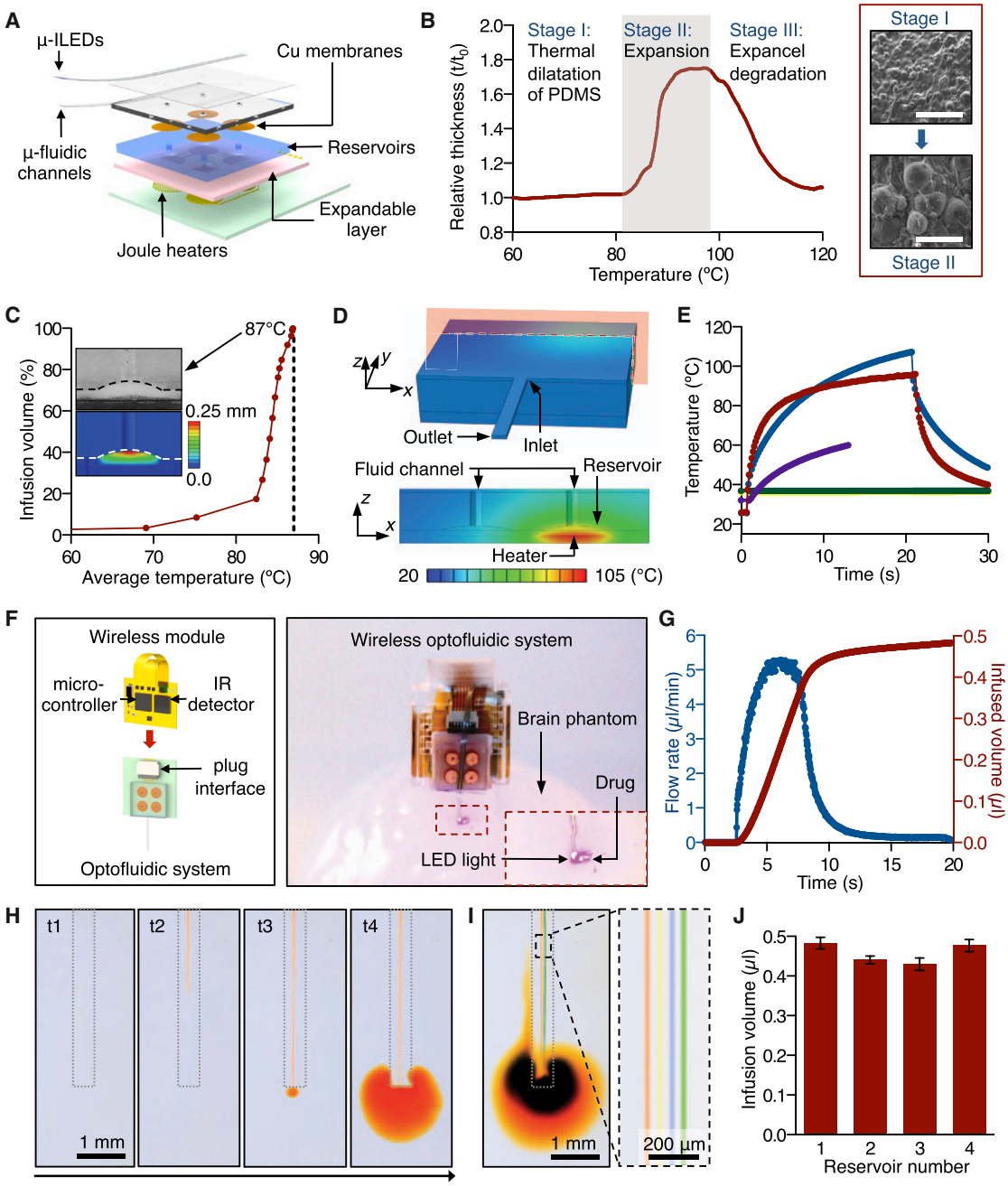

Figure 2. Thermo-Mechanical-Fluidic Characteristics of Wireless Optofluidic Systems

(A) Exploded view schematic diagram that illustrates an array of μ-ILEDs mounted on top of a soft microfluidic system that includes four separate microfluidic channels, each connected to a set of fluid reservoirs that include copper membranes as hermetic seals, expandable composite materials as mechanical transducers, and microscale Joule heating elements as actuators.

(B) Characteristics of a thermally expandable composite material. (Left) Thickness variation of this material as a function of temperature. (Right) SEM images (scale bar, 100 μm) show the expansion of microspheres upon application of heat at ~110°C.

(C) Dependence of the infused volume, as a percentage of the total volume of the reservoir, on temperature of the composite material. The dashed line indicates ~100% infusion at 87°C. (Inset top) Cross-sectional SEM image that shows complete filling of a reservoir with composite material by thermal expansion for a state of 100% infused volume. (Inset bottom) Corresponding distribution of vertical displacements in the composite material under the deformed configuration.

(D) Calculated temperature distribution at the surface of the entire three-dimensional computational model (top) and that at the cross-section defined by the red plane in the top (bottom).

(E) Computed (blue) and measured (red) temperature at the location of a thermal actuator immediately before, during, and after operation. The violet, green, and yellow curves correspond to calculations at the reservoir, the microfluidic inlet and outlet, respectively.

(legend continued on next page)

membranes (3 μm) seal the outlets of the reservoirs to prevent evaporation. This design allows delivery of multiple fluids without the repeated insertion of a delivery probe.

Activating a Joule heating element launches expansion of the corresponding active layer (Figure S2B). The resulting pressure in the reservoir ruptures the thin copper membrane and pumps the drug, with nearly 100% efficiency in volume delivery (0.5 μl in this case; Figure 2C), through the respective microfluidic channel. Quantitative measurements and numerical modeling (see Supplemental Experimental Procedures and Table S2 for details) based on finite element analyses (FEA) capture the thermal and mechanical aspects of operation. Because the modulus of the COP material (~2.6 GPa) is much higher than that of the expandable polymer (~3.0 MPa), deformations induced by thermal actuation are almost exclusively accommodated by the latter, as shown by both experimental and FEA results (Figures 2C, S2C, S2D, and S2F). Quantitative studies (Figure 2C) indicate a negligible amount (<8.5%) of infusion for heating of the active layer to temperatures below ~75°C, followed by a rapid increase above ~82°C, finally reaching complete infusion (>99.5% of the volume of the reservoir) at ~87°C. This nonlinear behavior originates from the nonlinear thermal expansion properties (Figure 2B). FEA results for the spatiotemporal temperature distribution of isolated Joule heating elements agree with IR images, as shown in Figure S2E, thereby validating the use of computation in design optimization (Figure S2G). The increase in temperature decays rapidly along both the thickness and in-plane directions (Figures 2D and S2H) to allow efficient individual control of the reservoirs. Computed and measured temperatures at representative locations for times before, during, and immediately after actuation appear in Figure 2E. The average temperature of the fluid in the reservoir remains in a range (< 60°C) compatible with many pharmacologically active compounds (Callahan et al., 2001; Joyce et al., 1984; Steger et al., 1996). Calculations based on a simplified fluid dynamics model (see Supplemental Experimental Procedures for details) indicate that the fluid cools significantly as it flows down the microfluidic channels before penetrating the targeted tissue (<0.1°C higher than the temperature of the surroundings). Therefore, this transient heating of the fluid does not appear deleterious to either the fluid or the tissue.

Figure 2F (left) provides a schematic illustration of control hardware and associated electronics, along with the key components that directly support the array of μ-ILEDs and the soft microfluidic probe. A battery-powered infrared (IR) wireless module enables independent control of fluid delivery and optical activation. The system uses serial communication between a separate IR transmitter (950 nm wavelength) and the receiver to provide programmable activation of individual heaters in the array (heater 1, 2, 3, or 4) and the μ-ILEDs (in this case 5, 10, 20, or 40 Hz with 10 ms pulse width; Figure S3A). A thin, flexible printed circuit board (PCB) serves as a substrate for a microcontroller (556-ATTINY84-20MU, Atmel), transistors, and an IR detector with wide sensing angle (120°; IR Sensor IC 38 kHz, Vishay Semiconductors). Two small, rechargeable lithium ion batteries (GM300910H, PowerStream Technology; Figure S3B) provide power. The entire collection of components (including the optofluidic probe, microfluidic reservoirs and actuators, the wireless module, and two batteries) is sufficiently lightweight (~1.8 g) to allow head mounting on adult mice and rats (Figure S3C). The wireless module and rechargeable batteries release from the optofluidics to allow quick replacement, thus facilitating long-term operation in various behavioral experiments.

Figure 2F (right) and Movie S1 demonstrate wireless operation of drug delivery and optical stimulation with a compact, self-contained device in a 3D-printed enclosure. Upon wireless triggering, the microcontroller activates a selected heater for drug delivery. The infusion rates non-linearly increase up to ~5.2 μl/min, such that most of the fluid is delivered within 13 s after initiating actuation (Figure 2G). The time dynamics of the expansion process and the geometries of the reservoirs and channels define these rates. Therefore, engineering the geometries of reservoirs and the dimensions of the channels can modulate the flow rate for different applications. Demonstration experiments using aqueous solutions of colored dyes and phantom brain tissue (0.6% agarose gel) verify these operational characteristics, as shown in Figures 2H and 2I and Movie S2. Figure 2J shows results for total volumes of fluid delivered from a set of reservoirs in a representative device. The observed wireless operational characteristics of these optofluidic probes offer powerful tools for integration with living neural tissue.

Optofluidic Devices Are Suitable for Wireless Pharmacology and Optical Manipulation in Awake, Behaving Animals

For application in vivo, the optofluidic drug delivery device can be chronically packaged with the platform for wirelessly triggered operation that includes infrared remote control, battery power, fluid reservoirs, and pumps with associated control electronics, all contained in a small head stage (Figures 3A and S5 and Movies S1, S2, and S3). To extend the lifetime of operation and reduce the impact on smaller organisms, the packaged electronics for the optofluidic device can be acutely affixed to an

(F) Complete wireless optofluidic system. (Left) Schematic illustration of the electronics, power, and wireless control system that plugs into the construct shown in Figure 2A. (Right) Demonstration of wireless drug delivery and optical stimulation by operation of the optofluidic system in a brain tissue phantom (0.6% agarose gel).

(G) Flow rate in a microfluidic channel (blue) and total infused volume (red) as a function of time before, during, and after actuation.

(H) Time sequence of optical images that demonstrates delivery of liquid (aqueous solution with orange dye) into brain phantom tissue (0.6% agarose gel) through a microfluidic channel: t1 = 0 s (onset of actuation), t2 = 3.1 s, t3 = 3.8 s, and t4 = 15.2 s.

(I) Images that show capabilities in separate delivery of different liquids (aqueous solutions with red, yellow, blue, and green dyes) through four individual microfluidic channels. The image on the right provides a magnified view.

(J) Total infusion volumes from each of four reservoirs in representative devices (average of three devices).

See also Figures S2, S3, S4 and Movies S1 and S2.

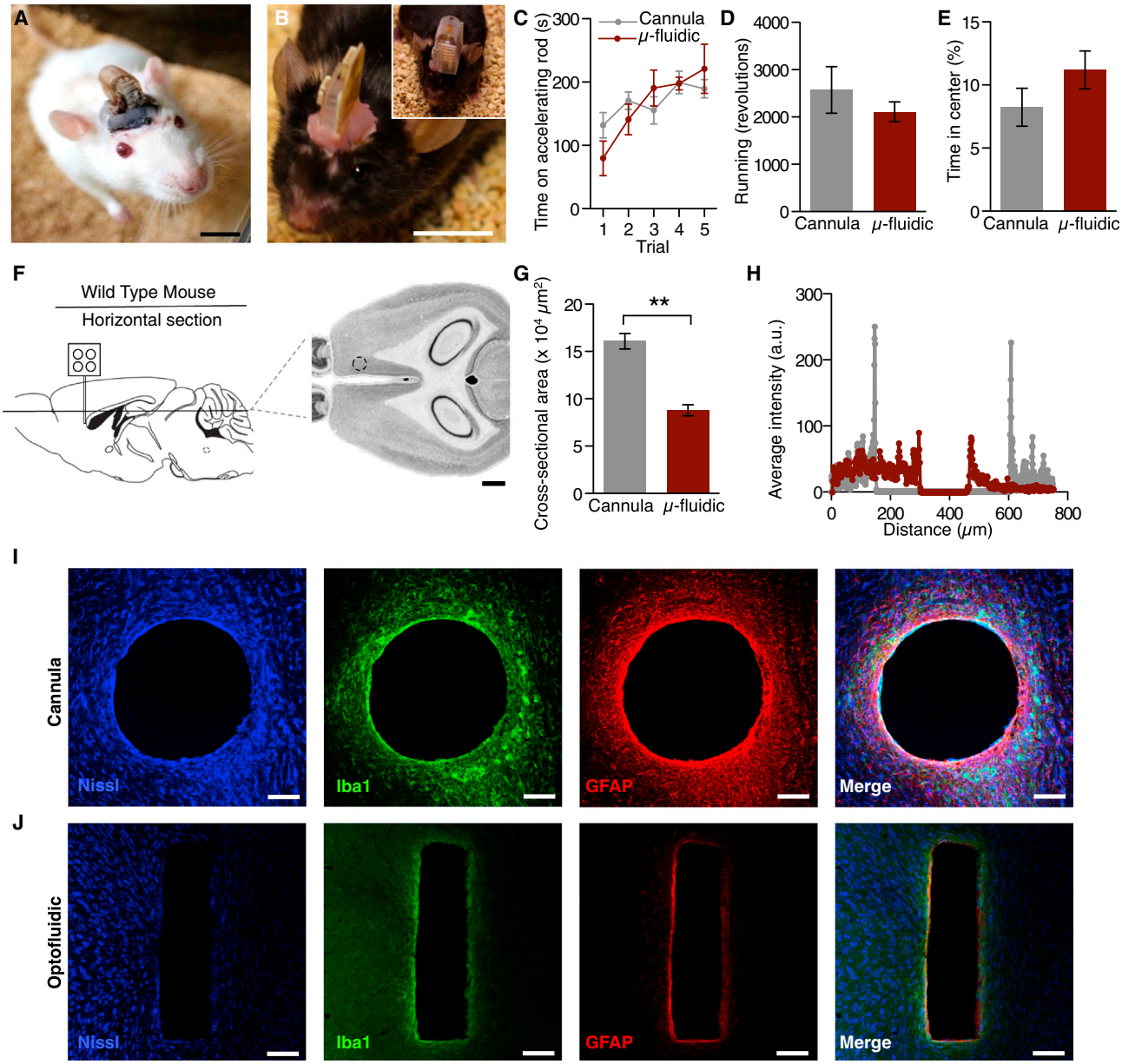

Figure 3. Optofluidic Devices Are Suitable for Wireless Pharmacology in Awake, Behaving Animals

(A and B) Images of a freely behaving (A) Sprague-Dawley rat and (B) a C57Bl6 mouse mounted with wireless power systems that are capable of drug delivery and photostimulation deep into brain tissue. All animals are healthy and freely moving, shown here 1 week following surgery. Scale bars, 1 cm.

(C–E) Wild-type (C57Bl6) mice tolerate the microfluidic devices, as well as traditional cannulas, and do not exhibit any notable deficits in (C) motor coordination, (D) spontaneous locomotor activity, or (E) anxiety-like behavior.

(F) Schematic and Mouse Brain Library atlas image of histological approach for inflammation and lesion study. Dashed circle indicates approximate injection site. Scale bar, 1 mm.

(G) Mean ± SEM cross-sectional area of lesions from cannulas and optofluidic probes (Student's t test, $^{**}p < 0.01$, n = 3/group).

(H) Representative linescan of fluorescence intensity from cannula (gray) and optofluidic probe (red) lesions.

(I and J) Representative confocal fluorescence images of 30 μm horizontal striatal slices show immunohistochemical staining for Nissl bodies (blue), astrocytes (GFAP, red), and activated microglia (Iba1, green) and overall lesion from a cannula (I) and an optofluidic device. All histological and confocal settings were kept consistent across groups. (J) In the rightmost panels, the shape and scale of the lesion from the cannula or optofluidic device is overlaid on the image of the other device (dashed lines). Scale bars, 100 μm. See also Figure S5 and Movie S3.

awake animal for acute device operation (Figure 3B). Mice with the fully encapsulated, chronically implanted wireless optofluidic devices interfaced to the dorsal striatum perform the rotarod test of sensorimotor control equally as well as cannula-implanted controls (Figures 3C and S5H). Also, when allowed to choose when and how to run on a wheel, optofluidic-implanted

mice run equally well as cannula-implanted controls (Figures 3D and S5I). Furthermore, chronic implantation does not alter anxiety-like behavior in the open field test (Figure 3E), an indication that bearing the device is not inherently stressful. These results indicate that even small mammals such as mice tolerate the chronically implanted probes equally as well as mice with conventional cannulas targeting the same brain structure. It is important to note that the cannulated mice in these experiments were not connected to an external drug supply. Such tethering can further restrict movement and negatively impacts performance on these tests, whereas the optofluidic-device-implanted mice are fully integrated with both the device and the fluid supply. In addition to comparable behavioral responses, the mechanical compliance and smaller overall tissue displacement of the microfluidic channels reduce lesioning and immunoreactive glial responses from deep brain implantation (Figures 3F–3J and Table S3). Additionally, the optofluidic devices provide access to four channels of drug, viral, or other fluid administration compared to a single channel for the cannula in a significantly smaller cross-sectional area (Figure 3G) of the brain. These thin, flexible optofluidic neural probes are better tolerated by the brain than rigid implants, consistent with previous reports of ultrathin, flexible deep brain implants (Canales et al., 2015; Capadona et al., 2012; Kim et al., 2013b; Kozai and Kipke, 2009; Kozai et al., 2012).

Wireless Virally Mediated Recombination and Visualization of Fluid Delivery

As a demonstration of the optofluidic probes' ability to deliver multiple, independent fluids through a single implant in an awake, behaving animal, we loaded two reservoirs with two different adeno-associated viruses to allow for recombination-dependent fluorescent visualization of successful fluid ejection. First, we delivered a virus expressing Cre recombinase (AAV5-PGK-Cre) into the dorsal striatum of a Cre-conditional tdTomato reporter mouse line (Ai9) developed by the Allen Institute for Brain Science (Figure 4A) (Madisen et al., 2010). We observed robust Cre-dependent expression of tdTomato in a distinct radius below the ventral tip of the microfluidic channels, thereby indicating efficient remote-controlled, virally induced in vivo recombination (Figure 4A). When we counted the number of tdTomato$^+$ cells emanating from the tip of the implant, we found the majority of the Cre-induced fluorescent reporter expression to be within 500 μm of the injection site (Figure 4B). Next, in a separate group of animals, we delivered the same AAV5-PGK-Cre, as well as a Cre-dependent eYFP reporter virus (AAV5-Ef1α-DIO-eYFP). In these animals, we clearly observed co-expression of both tdTomato and eYFP (Figures 4C–4E), indicating successful, combinatorial viral-mediated recombination in vivo. These are proof-of-principle experiments, but the same approach could be used to wirelessly alter gene expression at multiple time points without the need for multiple, disruptive surgeries or physical connection to viral infusion hardware. Together, these results further demonstrate that the optofluidic neural probes can be used for in vivo remote-controlled, independent delivery of fluids within an isolated region through individual and distinct channels running along a single implant.

Untethered, Programmed Pharmacological Infusion Alters the Behavior of Freely Moving Animals

The capability to load a single device with multiple fluids for independent, remote-controlled delivery offers the user the advantage of either multiplexed treatments or easily controlled within-subject study designs. As a demonstration of the latter, we implanted microfluidic devices unilaterally into the ventral tegmental area (VTA) of wild-type (C57Bl6) mice. Previous reports have demonstrated a remarkably stereotyped rotation behavior to unilateral μ-opioid receptor (MOPR) activation in the VTA (Devine and Wise, 1994; Jenck et al., 1988). As a proof-of-principle within-subject in vivo pharmacology experiment, two chambers of each device were loaded with different pharmacological agents—one with the synthetic opioid peptide and MOPR agonist [D-Ala^2, N-MePhe^4, Gly-ol]-enkephalin (DAMGO, 200 pmol, Tocris) and one with artificial cerebral spinal fluid (ACSF) as a vehicle control. In a counter-balanced design, we then wirelessly delivered either the DAMGO or vehicle into the VTA of freely behaving animals over a distance of ~1 m away from the animal (Figures 5A and 5B). Consistent with previous reports (Calenco-Choukroun et al., 1991; Devine and Wise, 1994; Jenck et al., 1988; Latimer et al., 1987), when DAMGO was infused into the VTA, the animals showed a robust increase in overall locomotor activity (Figures 5C–5E). In particular, the unilateral administration causes stereotypical rotations contralateral to injection site that is completely absent when the same animals receive the wireless ACSF infusion (Figures 5B, 5C, and 5E). This experiment demonstrates the utility of the optofluidic probes for self-contained, within-subject experiments to wirelessly deliver multiple chemicals into the brain without any physical contact with the animal for unconstrained freely moving behavior.

Concomitant Wireless Photostimulation with Wireless Pharmacological Antagonism Modulates a Dopaminergic Real-Time Place Preference

We next determined the in vivo optofluidic capabilities of these devices. Real-time place preference has become a common tool for neuroscientists to assess the behavioral valence of photostimulated neural circuits or cell bodies in a freely moving animal (Jennings et al., 2013; Kim et al., 2013a; Siuda et al., 2015; Stamatakis and Stuber, 2012; Stamatakis et al., 2013; Tan et al., 2012). In related behavioral models, phasic optogenetic activation of VTA dopaminergic (VTA-DA) neurons is rewarding (Kim et al., 2012, 2013b; Tsai et al., 2009; Witten et al., 2011). However, we previously failed to observe that wireless phasic activation of VTA-DA cell bodies was sufficient for a real-time place preference (Kim et al., 2013b). Because of the pronounced heterogeneity of VTA projections (Gunaydin et al., 2014; Lammel et al., 2011, 2012, 2015; Stamatakis et al., 2013; Stuber et al., 2015), we sought to selectively target VTA-DA projections into the shell of the nucleus accumbens (NAcSh). To do this, we selectively targeted channelrhodopsin-2 fused with eYFP (AAV5-EF1a-ChR2(H134)-eYFP) to VTA-DA neurons of TH-Cre mice and implanted an integrated optofluidic probe adjacent to the NAcSh (Figures 6A, 6B, and S6A–S6C). In this experiment, we found that photostimulation of the NAcSh-projecting VTA-DA fibers resulted in an increase in c-*fos* expression, a

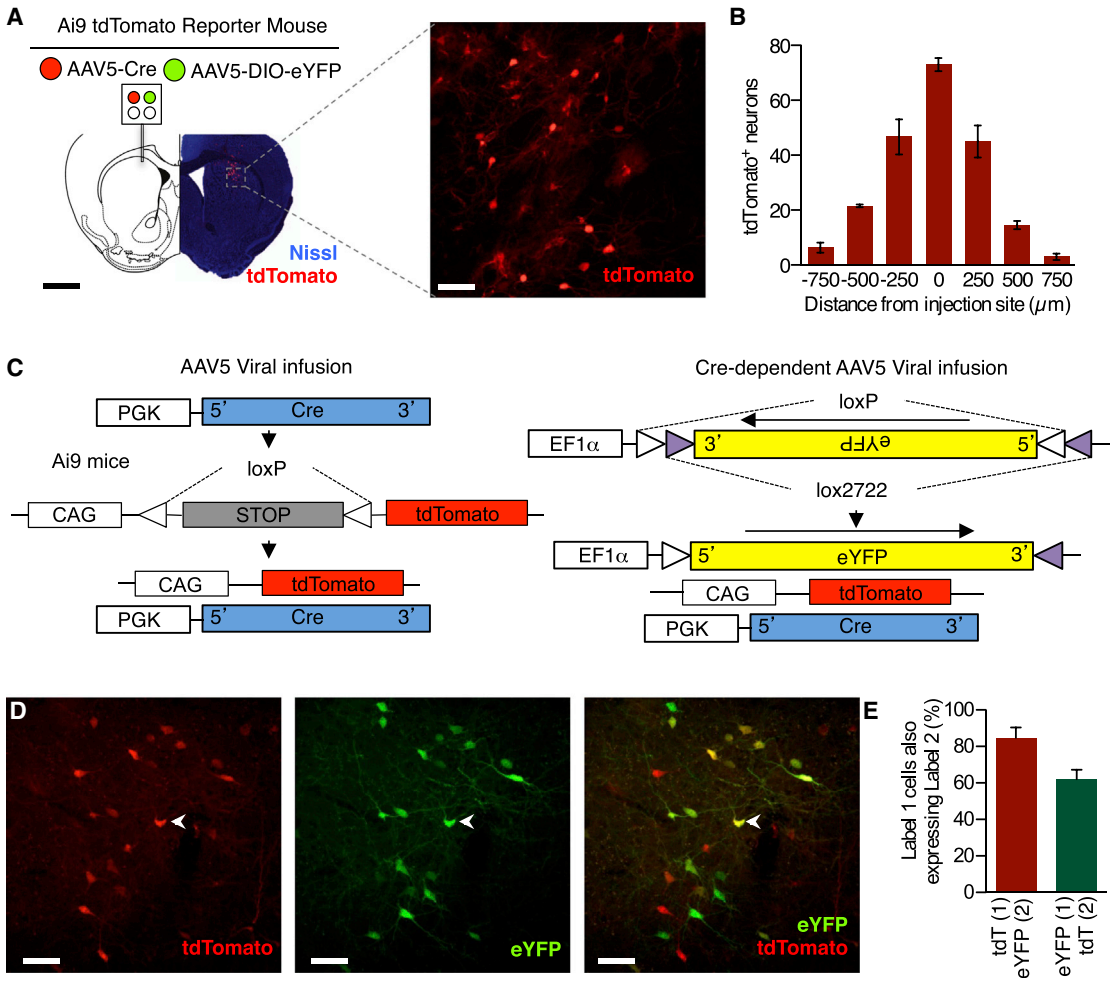

Figure 4. Wireless Virally Mediated Recombination Visualizes the Spread of Fluid Delivery

(A) Schematic of viral delivery experiment depicting loading of two distinct viruses into a single microfluidic device; fluorescence image depicts bolus of Cre-mediated recombination (imaged as expressed tdTomato, red; Nissl, blue) near the tip of the implanted microfluidic device. Right, enlarged maximum projection of 35 confocal fluorescence images (tdTomato, red). Black scale bar, 1 mm; white scale bar, 25 μm.

(B) Quantification of the spread of AAV5-PGK-Cre viral recombination. Cells counted in serial coronal slices from point of infusion (n = 3 slices per brain from 3 brains).

(C) Viral recombination scheme for the dual viral approach taken in (D) and (E).

(D) Representative maximum projection of 35 confocal fluorescence images of 30 μm coronal striatal slices demonstrates efficient virally induced gene expression (left-tdTomato, red; middle - eYFP, green, right-overlay) following wireless delivery of viruses. Chevron indicates example co-localization of tdTomato and eYFP. Scale bar, 25 μm.

(E) Quantification of co-localization of tdTomato (tdT) and eYFP (n = 3 slices per brain from 3 brains).

widely used biochemical marker of neuronal activation, in both the accumbens and the ventral tegmental area (presumably through antidromic activation) (Figures S6D and S6E and Table S3). To test whether any of the observed behavioral phenotypes were dopamine dependent, we filled one chamber of the optofluidic device with the selective dopamine receptor D_1 (DRD1) antagonist SCH23390 (400 ng, Tocris) (Billard et al., 1984; Gunaydin et al., 2014; Hyttel, 1983). We found that phasic photostimulation (8 × 10 ms light pulses at 20 Hz every 5 s) of VTA-NAcSh terminals was able to drive a robust real-time place preference (Figures 6C and 6D). Importantly, in a counterbalanced design, this place preference was completely blocked by wireless pharmacological delivery of SCH23390 prior to photostimulation in the real-time place preference task, indicating that optogenetically induced dopamine release into the NAcSh elicits the real-time place preference via DRD1 activation. There was no effect of either the photostimulation or the drug treatment on TH-Cre^- control animals that did not express ChR2(H134)-eYFP (Figures 6E and 6F), and no treatment group displayed a significant effect on locomotor activity (Figure 6G). These findings demonstrate that completely self-contained, remote-controlled optofluidic neural probes can be easily incorporated into optogenetic studies to introduce pharmacological agents into the immediate region of targeted photostimulation

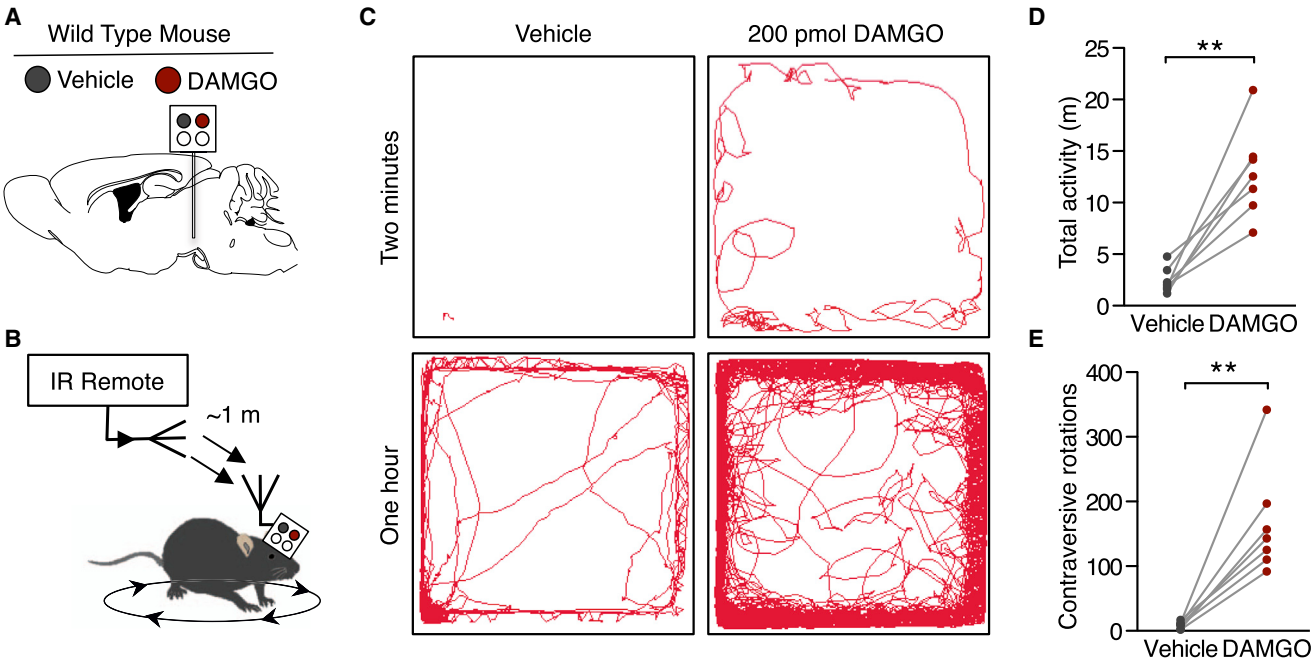

Figure 5. Untethered Delivery of Mu-Opioids into the Ventral Tegmental Area Causes Stereotypical, Repeated Rotation Behavior

(A) Schematic of the opioid peptide delivery experiment depicting loading of an agonist (200 pmol DAMGO, Tocris) and its vehicle into single microfluidic device.

(B) Cartoon of wireless scheme for the DAMGO-induced rotation experiment.

(C) Representative traces of movement from the same animal over the course of 2 min and 1 hr clearly show an increase in overall movement and rotations.

(D and E) Within-subject, counter-balanced experiments demonstrate robust wireless, DAMGO-induced changes in ambulatory behavior. Intra-VTA DAMGO causes a significant increase in (D) overall locomotion and (E) contraversive 360° rotations ($n = 7$, paired Student's t test, $^{**}p < 0.01$).

in a programmed fashion that is time locked and dependent on the behavior.

DISCUSSION

The wireless optofluidic neural probes presented here represent a compelling technology for programmable drug delivery and optical manipulation of deep brain tissue in freely moving animals. The resulting device platform has multifunctional capabilities in a single, soft implant that provides powerful options for in vivo pharmacology and wireless optogenetics, many of which would be impossible to reproduce with conventional metal cannulas and/or optical fibers.

A key advantage of these systems is the spatial specificity inherent in the multimodal brain/device interface. Previous demonstrations of wireless drug delivery have focused on defuse infusion of drug into the subcutaneous space of rats and, recently, humans (Farra et al., 2012; Hoare et al., 2009, 2011; Timko et al., 2014). Although these devices are capable of on-demand fluid delivery, they are unable to couple to the types of microfluidic channels necessary for discrete, targeted fluid delivery into deep brain tissue. The wireless optofluidic probes reported here overcome this challenge with a single device that causes a single, static lesion to brain tissue, where fluids and photons arrive at precisely the same micro-region of the brain. This co-localization targets the same cells with both drugs and photostimulation. One interesting possibility is in delivery of viral vectors for expression of exogenous receptors (light-sensitive ion channels, receptors, pumps, etc. or DREADD receptors), ligands for these or endogenous receptors, and photostimulation all to the same brain region and cell population. The compact, self-contained construction eliminates the repeated micro-lesions associated with internal cannulas and the angled lesions associated with exterior fiber optics, dramatically reducing overall trauma to the brain (Figures 3F and 3G). This minimally invasive operation facilitates a within-subject experimental design, thereby reducing the number of animals one needs to account for the behavioral variability that arises from any significant disruption of brain tissue. The soft neural interfaces enabled by these ultrathin, compliant probes also create new opportunities for chronic neuroscience research and preclinical investigation, as demonstrated not only here but also in recent studies of other soft device technologies for use in the epidural space (Minev et al., 2015). Importantly, the materials and designs presented here represent significant advances over these and other neural interfaces, all of which rely on tethered operation and lack capabilities in both wireless operation and photostimulation (Table S1) (Canales et al., 2015; Minev et al., 2015; Spieth et al., 2012). An important perspective is that the platforms reported here can easily be adapted for a wide range of other types of passive or active electronics technologies, including electrical microstimulation.

For any configuration, the value of the technology to the community depends on the extent to which it can be widely adopted. In this context, a relevant consideration is that the hardware for control and power management consists of readily available

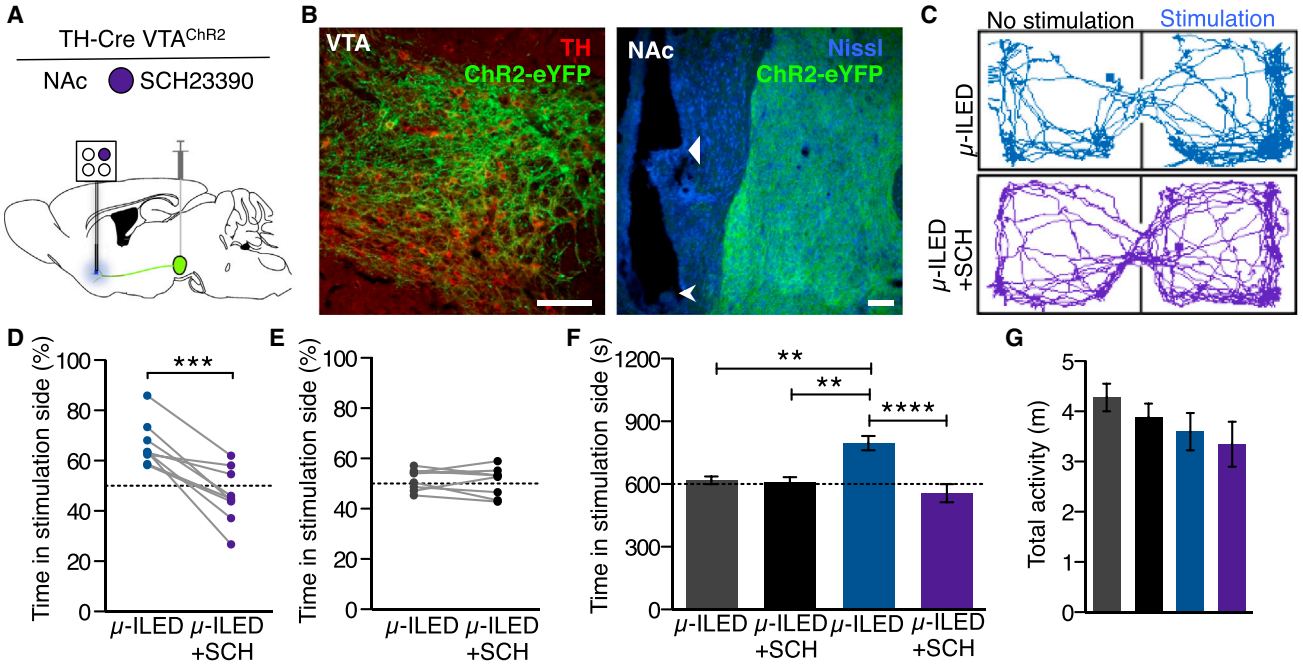

Figure 6. Wireless DRD1 Antagonism in the NAcSh Blocks Photostimulation-Induced Real-Time Preference of Freely Moving Animals

(A) Schematic of the optofluidic experiment. AAV5-EF1a-DIO-ChR2-eYFP was injected into the VTA, and 6 weeks later, an optofluidic probe loaded with SCH23390 (400 ng, Tocris) was implanted in the NAc of TH-Cre animals.

(B) Representative confocal fluorescence images depicting cell-type-specific expression of ChR2-eYFP in (right) dopaminergic, TH-containing neurons of the VTA (TH, red; ChR2-eYFP, green) and (left) their projections in the NAc (Nissl, blue; ChR2-eYFP, green). Triangular arrow indicates the ventral tip of the microfluidic channels, and the chevron indicates the ventral tip of the optofluidic device. All scale bars for the figure are 100 μm.

(C–G) Phasic photostimulation (8 pulses at 20 Hz, 10 ms pulse width upon entry and every 5 s the animal remains in the chamber) of NAc-projecting terminals from the VTA of TH-Cre animals drives a real-time place preference.

(C) Representative traces of movement during the real-time place testing experiment of one TH-Cre$^{VTA:ChR2}$ animal show a SCH23390-sensitive preference for the photostimulation-paired chamber.

(D) All TH-Cre$^{VTA:ChR2}$ animals show a real-time place preference that is significantly reduced following wireless intra-NAc delivery of SCH23390 (n = 9, paired Student's t test, ***$p < 0.001$).

(E) In Cre^{-} control animals, neither the photostimulation nor the SCH23390 treatment affects real-time preference behavior (n = 8, paired Student's t test, $p = 0.6234$).

(F) Grouped analysis confirms that the SCH23390-sensitive place preference is selective for the TH-Cre^{+} animals (n = 8–9/group, one-way ANOVA, Bonferroni Post hoc, **$p < 0.01$, ****$p < 0.0001$).

(G) There is no significant difference between any groups for overall locomotor activity (n = 8–9/group, one-way ANOVA).

See also Figure S6.

electronics hobbyist components (Figures S3 and S4). Aside from a simple IR remote control, the animal carries a small IR receiver system with little observable impact on its behavior (Figure 3 and Movie S3). In fact, after the initial surgery to implant and secure the device to the skull, the experimental subject never needs to come in contact with a human again. Complete operation of these optofluidic neural probes, including delivery of up to four distinct pharmacological agents, viruses, or other fluids, as well as photostimulation, can all be achieved wirelessly in any domain through which the IR signal can pass.

Areas for further improvement include dynamic control of fluid flow. Although the reported devices provide for multiple delivery events, each operates with identical rates of infusion (Figure 2G). While the infusion rate of the probes presented here could be faster than ideal for some desired applications, we did not directly observe any deleterious effects to either tissue or behavior associated with vehicle infusions. Nevertheless, engineered variations in the dimensions of the reservoirs and channels represent one means to define slower infusion rates and different flow conditions. Furthermore, care should be taken to ensure that the chosen fluids are compatible with delivery in these systems. Figure 2E demonstrates some transient heat transfer to the fluid prior to delivery. We purposefully chose to use potentially temperature-sensitive compounds (i.e., neuropeptides and viral vectors) and, in these cases, did not observe any limitations associated with delivery from these probes. However, it is important to empirically determine the thermal stability of each compound to be used in these systems. Another limitation is in refilling devices. With the current layouts, reuse of the microfluidics reservoirs and channels can be challenging. To overcome these restrictions, implementing replaceable fluid-containing cartridges (analogous to ink jet printer cartridges) might represent an attractive future design feature.

Even in existing embodiments, the device capabilities allow previously intractable experiments such as altering gene expression in freely behaving animals while living in their native home cage environments (Figures 4 and S5). The optofluidic neural probes can also provide photostimulation and delivery of pharmacological agents in a closed-loop manner based on the animals' behavior (Figures 6 and S6). Integration with real-time video acquisition of socially interacting animals (de Chaumont et al., 2012; Kunwar et al., 2015) would allow fully automated, programmed fluid delivery that could be tuned entirely to the social interactions of the animal. Beyond the possibilities in optogenetics, all of which require genetic modification, an interesting application could be in optopharmacology. The use of photosensitive compounds that act as photo-switches or ligands that bind to channels or receptors upon photo-conversion (Kramer et al., 2013) could exploit the high spatiotemporal control of both fluid and light delivery afforded by these optofluidic probes. Optopharmacological agents have been enthusiastically received in neuroscience for in vitro applications (Banghart and Sabatini, 2012; Callaway and Katz, 1993; Carter and Sabatini, 2004; Matsuzaki et al., 2001), but their use in vivo has been limited. Although compelling findings exist addressing the external visual nervous system and the surface of the cortex (Mourot et al., 2012; Noguchi et al., 2011; Polosukhina et al., 2012; Tochitsky et al., 2014), optopharmacological application in the deep brain remains a significant challenge. Optofluidic devices that provide access to the UV spectrum with advanced μ-ILEDs could target these highly selective photosensitive tools to spatially isolated regions of the central nervous system in non-genetically altered mammals.

Beyond basic research, the operation and architecture of the probes reported here will allow for a smooth translation to non-human primate models, as well as applications in clinical medicine. Therapeutic solutions for a diverse set of pathologies (e.g., local neurooncotherapy, pharmacologically refined deep brain stimulation, delivery of agents to mitigate traumatic brain injury, etc.) will benefit from the untethered and fully contained, programmable operation of devices similar in design to these optofluidic neural probes. Such centrally targeted drug delivery holds the promise of more tissue- and cell-type-selective therapies that avoid perturbing off-target organ systems. With these exciting future directions in mind, the results of our studies establish strategies for minimally invasive, ultrathin wireless optofluidic neural probes that can serve as a starting point for new generations of fluid neural interfaces.

EXPERIMENTAL PROCEDURES

Fabrication of Ultrathin, Flexible Optofluidic Probes

Fabrication of flexible microfluidic probes started with creating microfluidic channel patterns in a 25 μm PDMS layer (Sylgard 184, Dow Corning) using a molding process. For the mold, photo-curable epoxy (SU-8 10, Microchem) was spin coated (3,000 rpm for 10 μm) on a silicon wafer and UV exposed (120 mJ/cm^2) through a mask pattern. Removing the unexposed region by developing, followed by thermal annealing (65°C, 2 min – 75°C, 2 min – 85°C, 2 min – 95°C, 5 min – 65°C, 2 min), completed the fluidic channel mold. To facilitate release of patterned PDMS from the mold, it was chemically treated with evaporated anti-stiction agent (chlorotrimethylsilane, Sigma-Aldrich) for 20 min. PDMS was cast on the mold and pressed with a glass slide (5 × 3.5 cm^2) that was treated with Pt inhibitor solution (5% AEAPS (3-(2-Aminoethylamino) Propylmethyldimethoxysilane, Sigma-Aldrich) and 95% methanol) for 45 min; this inhibitor treatment facilitated release of the PDMS layer from the glass slide by deactivating Pt at the glass-PDMS interface. The glass slide and the mold were clamped, the PDMS between them was cured for 50 min at 70°C, and the glass slide with the patterned thin PDMS layer was detached from the Si mold.

A flat, thin PDMS layer (20 μm) was also prepared by spin-casting PDMS (2,000 rpm for 60 s) on a polycarbonate (PC) membrane and cured at 70°C for 1 hr. Both this flat PDMS layer on the PC membrane and the patterned PDMS layer on the glass slide were oxygen plasma-treated to activate their surfaces and bonded together to form microfluidic probes. After removing the PC membrane, the probes were released from the glass slide without damage due to the Pt inhibitor treatment of the glass surface. See the Supplemental Experimental Procedures for fabrication details of the μ-ILED array (Kim et al., 2013b; McCall et al., 2013). The μ-ILED array was integrated onto the microfluidic probe with double-sided adhesive (25 μm; ARclear 8154, Adhesives Research).

Fabrication of Optofluidic Drug Delivery Devices with Thermal Actuators

Heater patterns were photolithographically defined on Cr/Au (5 nm/185 nm) deposited FR-4 substrates (G10 glass epoxy sheet, ePlastics). The expandable layer (250 μm) was prepared on top of heaters on the FR-4 substrate by spin coating thermally expandable polymer (2:1 mixture of PDMS [elastomer: curing agent = 10:1] and expandable microspheres [Expancel 031 DU 40, AkzoNobel]) and cured at 70°C for 12 hr. Hemispherical reservoirs patterned in COP were aligned on the heaters and bonded using the double-sided adhesive. Parylene C (6 μm) was deposited on the inner walls of the reservoirs to further improve vapor impermeability and chemical resistance.

For fluid loading, the reservoirs were first treated with oxygen plasma (March RIE) for 30 s to make the inner surface hydrophilic. A syringe with a blunt needle was used to fill the reservoirs. To prevent fluid evaporation, the outlets of the reservoirs were hermetically sealed with Cu membranes (3 μm) after loading. Then, the inlets of an optofluidic probe were aligned and bonded with the outlets of the reservoirs.

Experimental Subjects

Adult (25–35 g) male C57BL/6J and TH::IRES-Cre backcrossed to C57BL/6J mice were group housed, given access to food pellets and water ad libitum, and maintained on a 12 hr:12 hr light:dark cycle (lights on at 7:00 AM). All mice were held in a facility in the lab 1 week prior to surgery, post-surgery and throughout the duration of the behavioral assays to minimize stress from transportation and disruption from foot traffic. Adult (275–325 g) male Lewis rats (LEW/CRL) were purchased from Charles River and housed in a climate-controlled facility with a 12:12 hr light-dark cycle under standard conditions. All procedures were approved by the Animal Care and Use Committee of Washington University and conformed to US NIH guidelines.

Implantation of Optofluidic Neural Probes

Soft, mechanically compliant optofluidic probes were implanted into the brain as previously described using thin (50 μm) stainless steel microneedles as insertion shuttles (Kim et al., 2013b; McCall et al., 2013). Water-soluble, purified silk (7 wt%) was used to bond an optofluidic probe to the microneedle, facilitating release of the microneedle after implantation. Figures S5A–S5E shows the sequential process of the surgery, and more detailed information can be found in the Supplemental Information.

Data Analysis/Statistics

Data are expressed as means ± SEM. Data were normally distributed, and differences between groups were determined using independent t tests or one-way ANOVA followed by post hoc Bonferroni comparisons if the main effect was significant at $p < 0.05$. Paired t tests were used in within subject design experiments. Statistical analyses were conducted using Prism 5.0 (GraphPad).

Device Availability

To inquire about wireless optofluidic device availability, please contact either of the corresponding authors via email.

SUPPLEMENTAL INFORMATION

Supplemental Information includes Supplemental Experimental Procedures, six figures, three tables, and three movies and can be found with this article online at http://dx.doi.org/10.1016/j.cell.2015.06.058.

AUTHOR CONTRIBUTIONS

Conceptualization, J.-W.J., J.G.M., M.R.B., and J.A.R. Methodology, J.-W.J., J.G.M., G.S., Y.Z., R.A., Y.H., M.R.B., and J.A.R. Software, J.-W.J. Formal analysis, J.-W.J., J.G.M., Y.Z., Y.S. Investigation, J.-W.J., J.G.M., G.S., Y.Z., R.A., M.K., S.L., J.Y.S., K.-I.J., D.Y.H., Y.L., G.P.S., L.X., and P.G. Resources, W.Z.R. Writing – Original Draft, J.-W.J., J.G.M., Y.Z., Y.H., M.R.B, and J.A.R. Writing – Review & Editing, J.-W.J., J.G.M., M.R.B, and J.A.R. Funding acquisition, M.R.B. and J.A.R. Supervision, Y.H. Project administration, M.R.B., and J.A.R.

ACKNOWLEDGMENTS

This material is based on work supported by the EUREKA NIDA R01DA037152 (M.R.B.), NIMH F31 MH101956 (J.G.M.), and NIDA K99DA038725 (to R.A.). We thank the Bruchas laboratory and the laboratory of Dr. Robert W. Gereau IV, in particular Tayler Sheahan and Dr. Judith Golden (Washington University) for helpful discussion. We thank Dr. Karl Deisseroth (Stanford University) for the channelrhodopsin-2 (H134), Dr. Garret Stuber (UNC) for the TH-IRES-Cre mice, the WUSTL Hope Center Viral Vector Core for viral packaging, and the WUSTL Pain Center for use of the rotarod and running wheels. All biomedical aspects of the device work were supported by a National Security Science and Engineering Faculty Fellowship of Energy (J.A.R.). The LED development was enabled by funding from the US Department of Energy, Division of Materials Sciences under award number DE-FG02-07ER46471 (J.A.R.), the NIH Common Fund NINDS R01NS081707 (J.A.R. and M.R.B.), and through the Materials Research Laboratory and Center for Microanalysis of Materials (DE-FG02-07ER46453) (J.A.R.).

Received: March 28, 2015
Revised: May 21, 2015
Accepted: June 2, 2015
Published: July 16, 2015

REFERENCES

Banghart, M.R., and Sabatini, B.L. (2012). Photoactivatable neuropeptides for spatiotemporally precise delivery of opioids in neural tissue. Neuron *73*, 249–259.

Billard, W., Ruperto, V., Crosby, G., Iorio, L.C., and Barnett, A. (1984). Characterization of the binding of 3H-SCH 23390, a selective D-1 receptor antagonist ligand, in rat striatum. Life Sci. *35*, 1885–1893.

Calenco-Choukroun, G., Daugé, V., Gacel, G., Féger, J., and Roques, B.P. (1991). Opioid delta agonists and endogenous enkephalins induce different emotional reactivity than mu agonists after injection in the rat ventral tegmental area. Psychopharmacology (Berl.) *103*, 493–502.

Callahan, W.J., Narhi, L.O., Kosky, A.A., and Treuheit, M.J. (2001). Sodium chloride enhances the storage and conformational stability of BDNF and PEG-BDNF. Pharm. Res. *18*, 261–266.

Callaway, E.M., and Katz, L.C. (1993). Photostimulation using caged glutamate reveals functional circuitry in living brain slices. Proc. Natl. Acad. Sci. USA *90*, 7661–7665.

Canales, A., Jia, X., Froriep, U.P., Koppes, R.A., Tringides, C.M., Selvidge, J., Lu, C., Hou, C., Wei, L., Fink, Y., and Anikeeva, P. (2015). Multifunctional fibers for simultaneous optical, electrical and chemical interrogation of neural circuits in vivo. Nat. Biotechnol. *33*, 277–284.

Capadona, J.R., Tyler, D.J., Zorman, C.A., Rowan, S.J., and Weder, C. (2012). Mechanically adaptive nanocomposites for neural interfacing. MRS Bull. *37*, 581–589.

Carter, A.G., and Sabatini, B.L. (2004). State-dependent calcium signaling in dendritic spines of striatal medium spiny neurons. Neuron *44*, 483–493.

Creed, M., Pascoli, V.J., and Lüscher, C. (2015). Addiction therapy. Refining deep brain stimulation to emulate optogenetic treatment of synaptic pathology. Science *347*, 659–664.

de Chaumont, F., Coura, R.D.-S., Serreau, P., Cressant, A., Chabout, J., Granon, S., and Olivo-Marin, J.-C. (2012). Computerized video analysis of social interactions in mice. Nat. Methods *9*, 410–417.

Devine, D.P., and Wise, R.A. (1994). Self-administration of morphine, DAMGO, and DPDPE into the ventral tegmental area of rats. J. Neurosci. *14*, 1978–1984.

Farra, R., Sheppard, N.F., McCabe, L., Neer, R.M., Anderson, J.M., Santini, J.T., Cima, M.J., and Langer, R. (2012). First-in-human testing of a wirelessly controlled drug delivery microchip. Sci. Transl. Med. *4*, 122ra21.

Gilletti, A., and Muthuswamy, J. (2006). Brain micromotion around implants in the rodent somatosensory cortex. J. Neural Eng. *3*, 189–195.

Gunaydin, L.A., Grosenick, L., Finkelstein, J.C., Kauvar, I.V., Fenno, L.E., Adhikari, A., Lammel, S., Mirzabekov, J.J., Airan, R.D., Zalocusky, K.A., et al. (2014). Natural neural projection dynamics underlying social behavior. Cell *157*, 1535–1551.

Hoare, T., Santamaria, J., Goya, G.F., Irusta, S., Lin, D., Lau, S., Padera, R., Langer, R., and Kohane, D.S. (2009). A magnetically triggered composite membrane for on-demand drug delivery. Nano Lett. *9*, 3651–3657.

Hoare, T., Timko, B.P., Santamaria, J., Goya, G.F., Irusta, S., Lau, S., Stefanescu, C.F., Lin, D., Langer, R., and Kohane, D.S. (2011). Magnetically triggered nanocomposite membranes: a versatile platform for triggered drug release. Nano Lett. *11*, 1395–1400.

Hyttel, J. (1983). SCH 23390 - the first selective dopamine D-1 antagonist. Eur. J. Pharmacol. *91*, 153–154.

Jenck, F., Bozarth, M., and Wise, R.A. (1988). Contraversive circling induced by ventral tegmental microinjections of moderate doses of morphine and [D-Pen2, D-Pen5]enkephalin. Brain Res. *450*, 382–386.

Jennings, J.H., Sparta, D.R., Stamatakis, A.M., Ung, R.L., Pleil, K.E., Kash, T.L., and Stuber, G.D. (2013). Distinct extended amygdala circuits for divergent motivational states. Nature *496*, 224–228.

Jeong, J.-W., Shin, G., Park, S.I., Yu, K.J., Xu, L., and Rogers, J.A. (2015). Soft materials in neuroengineering for hard problems in neuroscience. Neuron *86*, 175–186.

Joyce, J.R., Bal, T.S., Ardrey, R.E., Stevens, H.M., and Moffat, A.C. (1984). The decomposition of benzodiazepines during analysis by capillary gas chromatography/mass spectrometry. Biomed. Mass Spectrom. *11*, 284–289.

Kim, K.M., Baratta, M.V., Yang, A., Lee, D., Boyden, E.S., and Fiorillo, C.D. (2012). Optogenetic mimicry of the transient activation of dopamine neurons by natural reward is sufficient for operant reinforcement. PLoS ONE *7*, e33612.

Kim, S.-Y., Adhikari, A., Lee, S.Y., Marshel, J.H., Kim, C.K., Mallory, C.S., Lo, M., Pak, S., Mattis, J., Lim, B.K., et al. (2013a). Diverging neural pathways assemble a behavioural state from separable features in anxiety. Nature *496*, 219–223.

Kim, T.I., McCall, J.G., Jung, Y.H., Huang, X., Siuda, E.R., Li, Y., Song, J., Song, Y.M., Pao, H.A., Kim, R.-H., et al. (2013b). Injectable, cellular-scale optoelectronics with applications for wireless optogenetics. Science *340*, 211–216.

Konermann, S., Brigham, M.D., Trevino, A.E., Hsu, P.D., Heidenreich, M., Cong, L., Platt, R.J., Scott, D.A., Church, G.M., and Zhang, F. (2013). Optical control of mammalian endogenous transcription and epigenetic states. Nature *500*, 472–476.

Kozai, T.D.Y., and Kipke, D.R. (2009). Insertion shuttle with carboxyl terminated self-assembled monolayer coatings for implanting flexible polymer neural probes in the brain. J. Neurosci. Methods *184*, 199–205.

Kozai, T.D.Y., Langhals, N.B., Patel, P.R., Deng, X., Zhang, H., Smith, K.L., Lahann, J., Kotov, N.A., and Kipke, D.R. (2012). Ultrasmall implantable composite microelectrodes with bioactive surfaces for chronic neural interfaces. Nat. Mater. *11*, 1065–1073.

Kramer, R.H., Mourot, A., and Adesnik, H. (2013). Optogenetic pharmacology for control of native neuronal signaling proteins. Nat. Neurosci. *16*, 816–823.

Kunwar, P.S., Zelikowsky, M., Remedios, R., Cai, H., Yilmaz, M., Meister, M., and Anderson, D.J. (2015). Ventromedial hypothalamic neurons control a defensive emotion state. eLife *4*, 06633.

Lammel, S., Ion, D.I., Roeper, J., and Malenka, R.C. (2011). Projection-specific modulation of dopamine neuron synapses by aversive and rewarding stimuli. Neuron *70*, 855–862.

Lammel, S., Lim, B.K., Ran, C., Huang, K.W., Betley, M.J., Tye, K.M., Deisseroth, K., and Malenka, R.C. (2012). Input-specific control of reward and aversion in the ventral tegmental area. Nature *491*, 212–217.

Lammel, S., Steinberg, E.E., Földy, C., Wall, N.R., Beier, K., Luo, L., and Malenka, R.C. (2015). Diversity of transgenic mouse models for selective targeting of midbrain dopamine neurons. Neuron *85*, 429–438.

Latimer, L.G., Duffy, P., and Kalivas, P.W. (1987). Mu opioid receptor involvement in enkephalin activation of dopamine neurons in the ventral tegmental area. J. Pharmacol. Exp. Ther. *241*, 328–337.

Lee, H., Bellamkonda, R.V., Sun, W., and Levenston, M.E. (2005). Biomechanical analysis of silicon microelectrode-induced strain in the brain. J. Neural Eng. *2*, 81–89.

Madisen, L., Zwingman, T.A., Sunkin, S.M., Oh, S.W., Zariwala, H.A., Gu, H., Ng, L.L., Palmiter, R.D., Hawrylycz, M.J., Jones, A.R., et al. (2010). A robust and high-throughput Cre reporting and characterization system for the whole mouse brain. Nat. Neurosci. *13*, 133–140.

Matsuzaki, M., Ellis-Davies, G.C., Nemoto, T., Miyashita, Y., Iino, M., and Kasai, H. (2001). Dendritic spine geometry is critical for AMPA receptor expression in hippocampal CA1 pyramidal neurons. Nat. Neurosci. *4*, 1086–1092.

McCall, J.G., Kim, T.I., Shin, G., Huang, X., Jung, Y.H., Al-Hasani, R., Omenetto, F.G., Bruchas, M.R., and Rogers, J.A. (2013). Fabrication and application of flexible, multimodal light-emitting devices for wireless optogenetics. Nat. Protoc. *8*, 2413–2428.

Minev, I.R., Musienko, P., Hirsch, A., Barraud, Q., Wenger, N., Moraud, E.M., Gandar, J., Capogrosso, M., Milekovic, T., Asboth, L., et al. (2015). Biomaterials. Electronic dura mater for long-term multimodal neural interfaces. Science *347*, 159–163.

Mourot, A., Fehrentz, T., Le Feuvre, Y., Smith, C.M., Herold, C., Dalkara, D., Nagy, F., Trauner, D., and Kramer, R.H. (2012). Rapid optical control of nociception with an ion-channel photoswitch. Nat. Methods *9*, 396–402.

Noguchi, J., Nagaoka, A., Watanabe, S., Ellis-Davies, G.C.R., Kitamura, K., Kano, M., Matsuzaki, M., and Kasai, H. (2011). In vivo two-photon uncaging of glutamate revealing the structure-function relationships of dendritic spines in the neocortex of adult mice. J. Physiol. *589*, 2447–2457.

Polosukhina, A., Litt, J., Tochitsky, I., Nemargut, J., Sychev, Y., De Kouchkovsky, I., Huang, T., Borges, K., Trauner, D., Van Gelder, R.N., and Kramer, R.H. (2012). Photochemical restoration of visual responses in blind mice. Neuron *75*, 271–282.

Polstein, L.R., and Gersbach, C.A. (2015). A light-inducible CRISPR-Cas9 system for control of endogenous gene activation. Nat. Chem. Biol. *11*, 198–200.

Siuda, E.R., Copits, B.A., Schmidt, M.J., Baird, M.A., Al-Hasani, R., Planer, W.J., Funderburk, S.C., McCall, J.G., Gereau, R.W., 4th, and Bruchas, M.R. (2015). Spatiotemporal control of opioid signaling and behavior. Neuron *86*, 923–935.

Spieth, S., Schumacher, A., Holtzman, T., Rich, P.D., Theobald, D.E., Dalley, J.W., Nouna, R., Messner, S., and Zengerle, R. (2012). An intra-cerebral drug delivery system for freely moving animals. Biomed. Microdevices *14*, 799–809.

Stamatakis, A.M., and Stuber, G.D. (2012). Activation of lateral habenula inputs to the ventral midbrain promotes behavioral avoidance. Nat. Neurosci. *15*, 1105–1107.

Stamatakis, A.M., Jennings, J.H., Ung, R.L., Blair, G.A., Weinberg, R.J., Neve, R.L., Boyce, F., Mattis, J., Ramakrishnan, C., Deisseroth, K., and Stuber, G.D. (2013). A unique population of ventral tegmental area neurons inhibits the lateral habenula to promote reward. Neuron *80*, 1039–1053.

Steger, P.J., Martinelli, E.F., and Mühlebach, S.F. (1996). Stability of high-dose morphine chloride injection upon heat sterilization: comparison of UV-spectroscopy and HPLC. J. Clin. Pharm. Ther. *21*, 73–78.

Stuber, G.D., Stamatakis, A.M., and Kantak, P.A. (2015). Considerations when using cre-driver rodent lines for studying ventral tegmental area circuitry. Neuron *85*, 439–445.

Subbaroyan, J., Martin, D.C., and Kipke, D.R. (2005). A finite-element model of the mechanical effects of implantable microelectrodes in the cerebral cortex. J. Neural Eng. *2*, 103–113.

Tan, K.R., Yvon, C., Turiault, M., Mirzabekov, J.J., Doehner, J., Labouèbe, G., Deisseroth, K., Tye, K.M., and Lüscher, C. (2012). GABA neurons of the VTA drive conditioned place aversion. Neuron *73*, 1173–1183.

Timko, B.P., Arruebo, M., Shankarappa, S.A., McAlvin, J.B., Okonkwo, O.S., Mizrahi, B., Stefanescu, C.F., Gomez, L., Zhu, J., Zhu, A., et al. (2014). Near-infrared-actuated devices for remotely controlled drug delivery. Proc. Natl. Acad. Sci. USA *111*, 1349–1354.

Tochitsky, I., Polosukhina, A., Degtyar, V.E., Gallerani, N., Smith, C.M., Friedman, A., Van Gelder, R.N., Trauner, D., Kaufer, D., and Kramer, R.H. (2014). Restoring visual function to blind mice with a photoswitch that exploits electrophysiological remodeling of retinal ganglion cells. Neuron *81*, 800–813.

Tsai, H.-C., Zhang, F., Adamantidis, A., Stuber, G.D., Bonci, A., de Lecea, L., and Deisseroth, K. (2009). Phasic firing in dopaminergic neurons is sufficient for behavioral conditioning. Science *324*, 1080–1084.

Tye, K.M., and Deisseroth, K. (2012). Optogenetic investigation of neural circuits underlying brain disease in animal models. Nat. Rev. Neurosci. *13*, 251–266.

Walsh, J.J., Friedman, A.K., Sun, H., Heller, E.A., Ku, S.M., Juarez, B., Burnham, V.L., Mazei-Robison, M.S., Ferguson, D., Golden, S.A., et al. (2014). Stress and CRF gate neural activation of BDNF in the mesolimbic reward pathway. Nat. Neurosci. *17*, 27–29.

Witten, I.B., Steinberg, E.E., Lee, S.Y., Davidson, T.J., Zalocusky, K.A., Brodsky, M., Yizhar, O., Cho, S.L., Gong, S., Ramakrishnan, C., et al. (2011). Recombinase-driver rat lines: tools, techniques, and optogenetic application to dopamine-mediated reinforcement. Neuron *72*, 721–733.

Wu, F., Tien, L., Chen, F., Kaplan, D., Berke, J., and Yoon, E. (2013). A multi-shank silk-backed parylene neural probe for reliable chronic recording. In 2013 Transducers Eurosensors XXVII: The 17th International Conference on Solid-State Sensors, Actuators and Microsystems (TRANSDUCERS EUROSENSORS XXVII), pp. 888–891.

Zhang, K., and Cui, B. (2015). Optogenetic control of intracellular signaling pathways. Trends Biotechnol. *33*, 92–100.